International Journal of Applied Power Engineering (IJAPE)
Vol. 9, No. 2, August 2020, pp. 173~192
ISSN: 2252-8792, DOI: 10.11591/ijape.v9.i2.pp173-192

Series active power filter supplied by fuel cell for mitigating power quality issues

Abdallah Ben Abdelkader, Othmane Abdelkhalek, Youssef Mouloudi, Mohamed Amine Hartani, Benabid Slimane
Faculty of Technology, University of Tahri Mohammed Bechar, Algeria

Article Info

Article history:

Received Nov 25, 2019
Revised Feb 19, 2020
Accepted Mar 3, 2020

Keywords:

DC-DC converters
DC link
Fuel cell
Maximum power point tracker
Pulse width modulation
Series active power filter

ABSTRACT

In this paper, the combination of the series active power filter (SAPF) with a fuel cell (FC) source is deliberated. The FC based on the SAPF aims to compensate voltage deviations or disturbances that occur in the system caused by power quality issues. The proposed system consists of a fuel cell source connected to the DC link through two DC-DC converters, the first extracts the maximum power of the FC source through pulse width modulation (PWM) signals generated from the maximum power point tracker (MPPT) controller. Thus, the second converter is used to regulate the high voltage side of the converter through closed control loops, in addition to a voltage source inverter (VSI) and a series injection transformer. Despite of fluctuations of the DC link during the compensation of the needed energy, MPPT and closed control loops generate PWM signals to the switching devices of DC-DC boost converters in order to extract maximum fuel cell power and to maintain the bus voltage within its limits and around its reference values respectively. The proposed topology is simulated in MATLAB/Simulink software, where simulation results show that the proposed FC based SAPF can efficiently reduce problems of voltage sags-wells and harmonics.

This is an open access article under the CC BY-SA license.

Corresponding Author:

Abdallah Ben Abdelkader,
Department of Electrical of Engineering,
Tahri Mohammed Bechar University,
BP 417 Route deKenadsa, 08000 Bechar, Algeria.
Email: Abdallahbenabdelkader@yahoo.fr.

1. INTRODUCTION

Given the demand of improving the power quality especially in industry, where the critical equipment and sensitive loads are widely used and their power supply should not interrupted. Here, uninterrupted, clean and regulated power supply is required when feeding loads that have important tasks. In other hand, most common voltage disturbances appear in alternative current appliances AC providing a reduction in voltage amplitude known as sag. Thus, sag and interruptions provide most of the industrial problems (90%) that affect their supply quality [1]. Other, swell problem is also among disturbances that affect the power quality, which is defined by a rising in voltage amplitude above its nominal value [2]. In addition, harmonic distortion can provide huge problems in the whole of the power conversion chain such as heating the system components, mechanical oscillations, unpredictable behavior of protecting devices, and may cause damage [3, 4].

Due to these problems, it is necessary to approve protecting devices and effective solution to solve such disturbances. In this paper, we focus on series active power filter SAPF in order to mitigate sag-swell and harmonics [5-8] that affect our system. SAPF have the same topology as the active filter, with an excellent dynamic capability to restore the load voltage to i nominal value within a few milliseconds as

well providing power disruption to the supplied loads. In other researches, the series topology aims to compensate the sag with active power [9]. In power quality domain, various papers has used classical and intelligent controllers in order to improve the stability, robustness and excellent dynamic response of the APFS as mentioned in [4, 10-12].

The series APF systems need certainty to provide active power into the power system to maintain the load voltage level during voltage sag. At the same time, the power flow in the series SAPF system has drastically increased during the source voltage sag. Thus, additional energy sources need to be added into the series APF system DC-link. However, FC can cause the negative effects on the existing power systems. That is, some potential problems might be occurred such as voltage variation, protection, harmonics, and personnel safety. The FC is interfaced in the AC and DC distributed system by using power electronic circuits. The DC voltage must be limited within an acceptable range during steady state and dynamic conditions by using suitable control strategies. This paper proposes a combined operation system of SAPF and fuel cell, which is connected to the dc link. The advantage of the proposed system over the SAPF is to compensate the voltage interruption, as well as the voltage sag, harmonics. The operation of the proposed system was verified through simulations with MATLAB/Simulink.

2. SYSTEM DESCRIPTION

The objective of this study is to supply the SAPF with a SOFC source through dc-dc boost converters to extract the maximum power of the FC and stabilize the output operating voltage of the DC link, while compensating voltage fluctuations. The module framework is shown in Figure 1, where a sensitive three-phase load is supplied by a three-phase source through a three-phase impedance. The injection mode of the SAPF is achieved through a three-phase transformer, where line voltages of the load are restored around its reference values during the applied voltage disturbance at the grid side. The storage unit can be replaced by the SOFC with its conversion chain as viewed in the Figure 1.

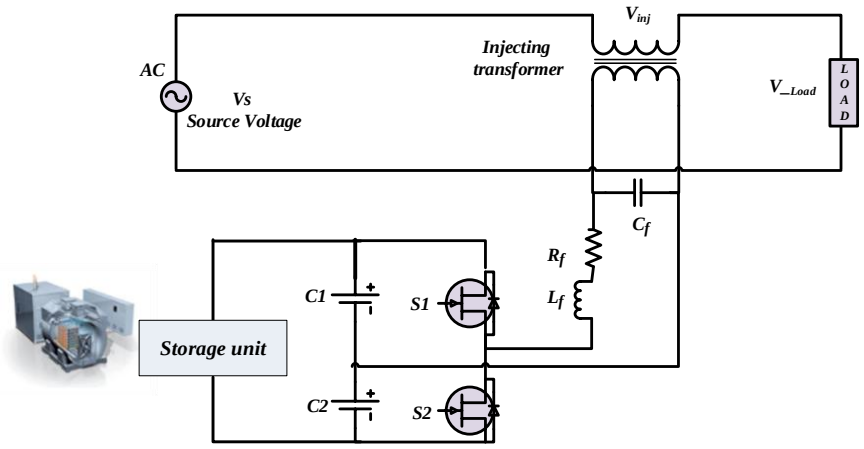


Figure 1. General configuration of the SAPF-FC system

2.1. Modeling and characteristics of SOFC

The operating principal of the FOFC device is based on the electrochemical reaction between hydrogen and oxygen across a solid electrolyte, in order to generate electricity. Exactly, the O^2 ions are constructed at the cathode side, where the oxygen accepts electrons from the load circuit. The produced ions are transferred afterward to the anode through the electrolyte, and then combined with hydrogen to form water. The results of this reaction are transferred through the load circuit to the cathode [13]. The essential reactions of the SOFC are the following, at the cathode:

$$O_2 + 4e^- \rightarrow 2O^{-2} \quad (1)$$

at the anode:

$$H_2 + O^{-2} \rightarrow H_2O + 2e^{-2} \quad (2)$$

the overall reaction is:

$$H_2 + 1/2O_2 \rightarrow H_2O \quad (3)$$

the dynamic model of the SOFC is detailed in references [13-18].

Following expression represents the output voltage of the stack device:

$$v_{fc} = (v_{nernst} - v_{ohm} - v_{act} - v_{conc}) \quad (4)$$

The ohmic losses V ohm is caused by electrical resistance of electrodes, the resistance to the flow of ions in the electrolyte, which can be deduced by Ohm's law.

2.1.1. Ohmic losses

These losses are due to the opposition of electrons through the anodes and to the relocation of particles through the electrolyte. In addition, the interconnections or bipolar plates of the FC source are added to the ohmic losses [13-15].

$$v_{ohm} = ri_{fc} \quad (5)$$

where *r* is the internal resistance and i_{fc} is the fuel cell stack current.

2.1.2. Activation losses

This loss is caused by the sluggishness of chemical reaction that takes place on the surface of electrodes. A drop voltage produced by the fuel cell is carrying the reaction forward, which transfers the electrons to or from the electrode [13]. The activation loss v_{act} is given by:

$$v_{act} = \frac{RT}{2\alpha F}\ln\left(\frac{i_{fc}}{i_{fcO}}\right) \quad (6)$$

where *R* is the ideal gas constant, *T* is the temperature, and *F* is the Faraday constant. The coefficient α represents the electron transfer of the reaction at the electrode, and i_{fc0} is the exchange current of the fuel cell stack.

2.1.3. Concentration losses

These losses are known as mass transport losses and are caused due to the reduction in the concentration of reactants in the region of the electrode when the fuel is consumed. The consumption of reactants at respective electrodes, i.e. hydrogen at the anode and oxygen at the cathode leads to a slight reduction in the reactants concentrations, which cause a drop in partial pressure of gases resulting in a drop voltage that portion of the electrode can produce [13]. The concentration loss v_{conc} is defined by (7):

$$v_{conc} = \frac{RT}{2F}\ln\left(1 - \frac{i_{fc}}{i_{fcO}}\right) \quad (7)$$

where ifcl is the limiting current.

The Nernst equation is:

$$v_{nernst} = v_{standard} - \frac{RT}{2F}\ln\left(\frac{P_{H_2}\sqrt{P_{O_2}}}{P_{H_2O}}\right) \quad (8)$$

where v standard is the open-circuit potential at the standard pressures. p_{H2} , p_{O2} and p_{H2O} are the partial pressure of hydrogen, oxygen and water respectively. Thus, these pressures are defined in (5), which are as follow:

$$\frac{dp_{H_2}}{dt} = -\frac{1}{\tau_{H_2}}p_{H_2} + \frac{1}{\tau_{H_2}K_{H_2}}\left(q_{H_2}^{in} - 2K_r i_{fc}\right) \quad (9)$$

$$\frac{dPO_2}{dt} = -\frac{1}{\tau_{O_2}}p_{O_2} + \frac{1}{\tau_{O_2}K_{O_2}}\left(q_{O_2}^{in} - 2K_r i_{fc}\right) \quad (10)$$

$$\frac{dp_{H_2O}}{dt} = -\frac{1}{\tau_{H_2O}}p_{H_2O} + \frac{1}{\tau_{H_2O}K_{H_2O}}2K_r i_{fc} \quad (11)$$

where τ_{H2} , $\tau_{O2}$and τ_{H2O} are fuel, air and fuel exhaust valves time constants respectively. Qin H2, qin H_2O are the input molar flows of hydrogen and water across the anode valve [kmol/s]. The constants KH_2, KO_2 and KH_2O are the valve molar for hydrogen, oxygen and water respectively [kmol/(s atm)]. For modeling purpose, a constant is defined by *Kr=N/4F*. The total generation of the fuel cell is:

$$p_{fc} = Nv_{fc}i_{fc}$$

2.2. Modeling and characteristics of SAPF

The control strategy used to extract the reference voltages of series active power filter (SAPF) is based on the PQ method [15, 19], and the control scheme is shown in Figure 2.

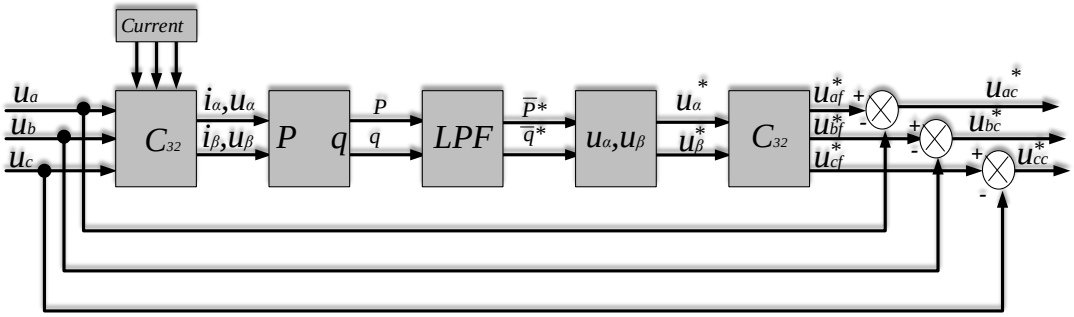


Figure 2. Series active power filter strategy control

The grid three-phase voltage source is assumed to be symmetric and not distorted:

$$\begin{bmatrix} u_a \\ u_b \\ u_c \end{bmatrix} = \begin{bmatrix} \sum_{n=1}^{\infty} \sqrt{2} U_n sin(n\omega t + \theta_n) \\ \sum_{n=1}^{\infty} \sqrt{2} U_n sin\left((n\omega t - \frac{2\pi}{3}) + \theta_n\right) \\ \sum_{n=1}^{\infty} \sqrt{2} U_n sin\left((n\omega t + \frac{2\pi}{3}) + \theta_n\right) \end{bmatrix} \quad (12)$$

where *Un* and *θn* are respectively the root mean square (rms) voltage and initial phase angle, *n* is the harmonic order. When *n=1*, it means three-phase fundamental voltage source.

$$\begin{bmatrix} u_{sa} \\ u_{sb} \\ u_{sc} \end{bmatrix} = \begin{bmatrix} \sqrt{2} U_1 sin\ (\omega t + \theta_1) \\ \sqrt{2} U_1 sin\ \left((\omega t - \frac{2\pi}{3}) + \theta_1\right) \\ \sqrt{2} U_1 sin\ \left((\omega t + \frac{2\pi}{3}) + \theta_1\right) \end{bmatrix} \quad (13)$$

The (12) is transformed into (α-β) reference frame,

$$\begin{bmatrix} u_\alpha \\ u_\beta \end{bmatrix} = C_{32} \begin{bmatrix} u_{sa} \\ u_{sb} \\ u_{sc} \end{bmatrix} = \sqrt{3} \begin{bmatrix} \sum_{n=1}^{\infty} U_n sin\ (n\omega t + \theta_n) \\ \sum_{n=1}^{\infty} \pm U_n sin\ (n\omega t + \theta_n) \end{bmatrix} \quad (14)$$

$$C_{32} = \sqrt{\frac{2}{3}} \begin{bmatrix} 1 & \frac{-1}{2} & \frac{-1}{2} \\ 0 & \frac{\sqrt{3}}{2} & \frac{-\sqrt{3}}{2} \end{bmatrix} \quad (15)$$

The three-phase positive fundamental current template is constructed as:

$$\begin{bmatrix} i_a \\ i_b \\ i_c \end{bmatrix} = \sqrt{\frac{2}{3}} \begin{bmatrix} sin\ (\omega t) \\ sin\ (\omega t - \frac{2\pi}{3}) \\ sin\ (\omega t + \frac{2\pi}{3}) \end{bmatrix} \quad (16)$$

The (16) is transformed to (α-β) reference frame:

$$\begin{bmatrix} i_\alpha \\ i_\beta \end{bmatrix} = C_{32} \begin{bmatrix} i_a \\ i_b \\ i_c \end{bmatrix} = \begin{bmatrix} sin\ (\omega t) \\ -cos\ (\omega t) \end{bmatrix} \quad (17)$$

According to the instantaneous reactive power theory [13], then:

$$\begin{bmatrix} p \\ q \end{bmatrix} = \begin{bmatrix} u_\alpha & u_\beta \\ u_\beta & -u_\alpha \end{bmatrix} \begin{bmatrix} i_\alpha \\ i_\beta \end{bmatrix} \quad (18)$$

where AC and DC components are included:

$$\begin{bmatrix} p \\ q \end{bmatrix} = \begin{bmatrix} \bar{p} + \tilde{p} \\ \bar{q} + \tilde{q} \end{bmatrix} \quad (19)$$

where p and q are passed through low pass-filter (LPF) and DC component is gotten by:

$$\begin{bmatrix} \bar{p} \\ \bar{q} \end{bmatrix} = \sqrt{3} \begin{bmatrix} U_1 cos\ (\theta_1) \\ U_1 sin\ (\theta_1) \end{bmatrix} \quad (20)$$

According to [15], transformation is made:

$$\begin{bmatrix} p \\ q \end{bmatrix} = \begin{bmatrix} u_\alpha & u_\beta \\ u_\beta & -u_\alpha \end{bmatrix} \begin{bmatrix} i_\alpha \\ i_\beta \end{bmatrix} = \begin{bmatrix} i_\alpha & i_\beta \\ -i_\beta & i_\alpha \end{bmatrix} \begin{bmatrix} u_\alpha \\ u_\beta \end{bmatrix} \quad (21)$$

The DC components of p and q:

$$\begin{bmatrix} \bar{p} \\ \bar{q} \end{bmatrix} = \begin{bmatrix} u_{\alpha f} & u_{\beta f} \\ u_{\beta f} & -u_{\alpha f} \end{bmatrix} \begin{bmatrix} i_\alpha \\ i_\beta \end{bmatrix} = \begin{bmatrix} i_\alpha & i_\beta \\ -i_\beta & i_\alpha \end{bmatrix} \begin{bmatrix} u_{\alpha f} \\ u_{\beta f} \end{bmatrix} \quad (22)$$

The fundamental voltages in (α-β) reference frame are:

$$\begin{bmatrix} u_{\alpha f} \\ u_{\beta f} \end{bmatrix} = \begin{bmatrix} i_\alpha & i_\beta \\ -i_\beta & i_\alpha \end{bmatrix}^{-1} \begin{bmatrix} \bar{p} \\ \bar{q} \end{bmatrix} = \begin{bmatrix} i_\alpha & -i_\beta \\ i_\beta & i_\alpha \end{bmatrix} \begin{bmatrix} \bar{p} \\ \bar{q} \end{bmatrix} \quad (23)$$

The three-phase fundamental voltages are specified by:

$$\begin{bmatrix} \mathrm{u_{af}} \\ \mathrm{u_{bf}} \\ \mathrm{u_cf} \end{bmatrix} = \mathrm{C_{23}} \begin{bmatrix} \mathrm{u_{\alpha f}} \\ \mathrm{u_{\beta f}} \end{bmatrix} = \sqrt{2}\mathrm{U_1} \begin{bmatrix} \sin\ (\omega t + \theta_1) \\ \sin\ (\omega t + \theta_1 - \frac{2\pi}{3}) \\ \sin\ (\omega t + \theta_1 + \frac{2\pi}{3}) \end{bmatrix} \quad (24)$$

where;

$$\mathrm{C_{23}} = \begin{bmatrix} 1 & 0 \\ -1/2 & \sqrt{3}/2 \\ -1/2 & \sqrt{3}/2 \end{bmatrix} \quad (25)$$

2.3. Modeling of DC-DC boost converter

DC-DC boost converter or step-up voltage converter, steps up input voltages, step down input currents of the DERs through the circuit as shown in Figure 3. V_{low} and V_{high} are the voltage at low and high voltage sides respectively and d(t) is the switching duty cycle. Generalized equations of the power converters can be derived for continuous conduction mode CCM due to its simplicity, where two states are used. Starting from the state space equations during the ON-OFF switching states, the converter model can be linearized using an averaging method. For the used dc-dc converters, when the switching device is turned on, it conducts for a ratio D of a period (26), and when the switching device is turned off, the diode conducts for a ratio of (1-D) of the same period (27).

$$\begin{cases} \dot{X} = A_{on}X + B_{on}Y \\ \begin{bmatrix} \dot{i_L} \\ \dot{V_c} \end{bmatrix} = \begin{bmatrix} 0 & 0 \\ 0 & -\frac{1}{RC} \end{bmatrix} \begin{bmatrix} i_L \\ V_c \end{bmatrix} + \begin{bmatrix} \frac{1}{L} \\ 0 \end{bmatrix} V_{in} \end{cases} \quad (26)$$

$$\begin{cases} \dot{X} = A_{off}X + B_{on}Y \\ \begin{bmatrix} \dot{i_L} \\ \dot{V_c} \end{bmatrix} = \begin{bmatrix} 0 & -\frac{1}{L} \\ \frac{1}{C} & -\frac{1}{RC} \end{bmatrix} \begin{bmatrix} i_L \\ V_c \end{bmatrix} + \begin{bmatrix} 0 \\ 0 \end{bmatrix} V_{in} \end{cases} \quad (27)$$

The (28) is used to linearize the above state-space equations of the buck converter, where X is the steady-state component and D is the steady state or DC component duty-ratio.

$$\dot{X} = [\overline{D}A_{on} + (1 - \overline{D})\, A_{off}]X + [\overline{D}B_{on} + (1 - \overline{D})\, B_{on}]Y \quad (28)$$

$$\begin{cases} \begin{bmatrix} \dot{i_L} \\ \dot{V_c} \end{bmatrix} = \begin{bmatrix} 0 & -\frac{1-D}{L} \\ \frac{1-D}{C} & -\frac{1}{RC} \end{bmatrix} \begin{bmatrix} i_L \\ V_c \end{bmatrix} + \begin{bmatrix} \frac{V_c}{L} \\ -\frac{i_L}{C} \end{bmatrix} d \end{cases} \quad (29)$$

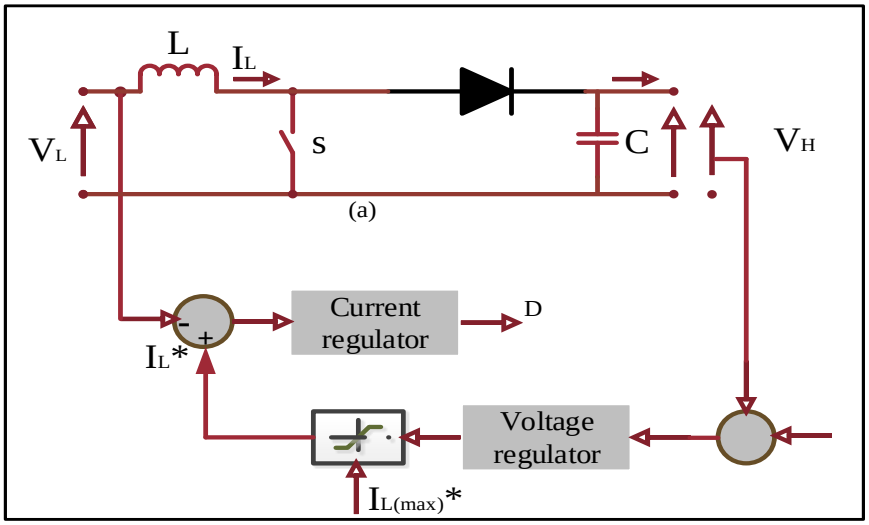


Figure 3. Closed loop boost converter circuit

2.3.1. Perturb and observe P&O

This MPPT method is the widely common and used due to its simplicity and its ease of implementation. Thus, this MPPT method perturbs the system variables (voltage and current), and consequently observes the output generation of the FC source. The principal of this technique is to adjust the operating voltage of the system around the maximum power point (ΔP=ΔV>0), (ΔP=ΔV<0). The mathematical expression that resumes the operating principal of the P&O algorithm is:

$$V(k) = V(k-1) + \Delta V.sign\left(\frac{dP}{dV}\middle|V = V_{k-1}\right) \quad (30)$$

The following Table 1 can illustrate the variation of this MPPT technique around the MPP operating point of the system.

Table. 1 Disturbances of V-P curve (ΔP/ΔV) of P&O MPPT technique

Disturbance	Change in the power	Next disturbance
Positive	Positive	Positive
Positive	Negative	Negative
Negative	Positive	Negative
Negative	Negative	Positive

3. RESULTS AND ANALYSIS

In this section, MATLAB/Simulink simulation results are presented and discussed in details. The proposed SAPF-FC model is simulated by MATLAB/Simulink as shown in Figure 4. Thus, five phenomena are studied in this paper, where the SAPF with the SOFC compensate disturbances of the voltage that appear across the source to avoid damage of the connected load. Such disturbances are applied by a programmable AC source, which is defined by the following specifications:

– Root mean square RMS of the phase-phase voltage: 380 V
– Phase angle: 0°
– Frequency: 50Hz

Next section deals with a discussion of the applied phenomenon independently.

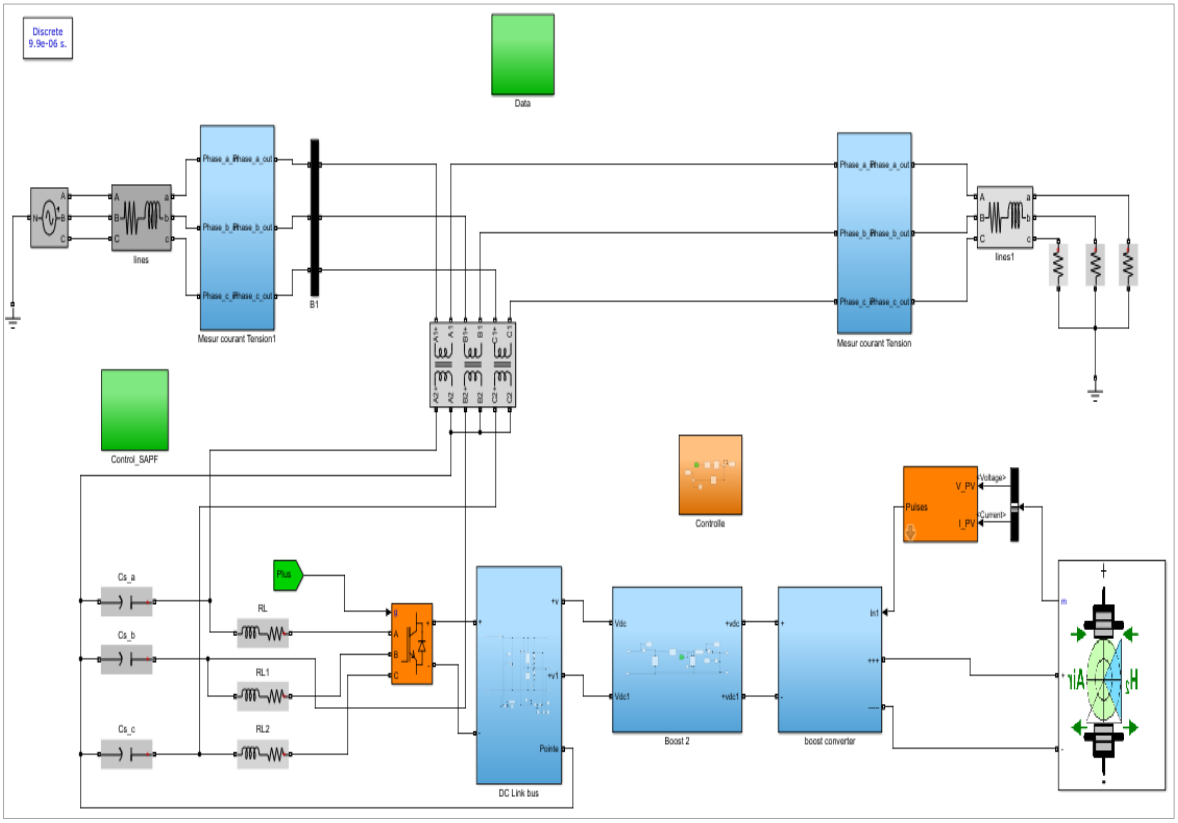
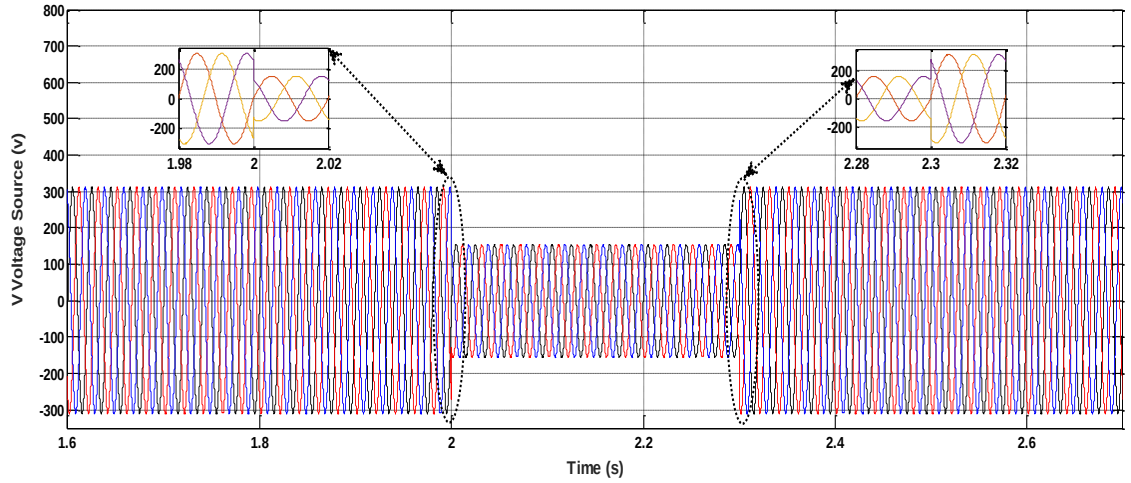


Figure 4. System synoptic scheme

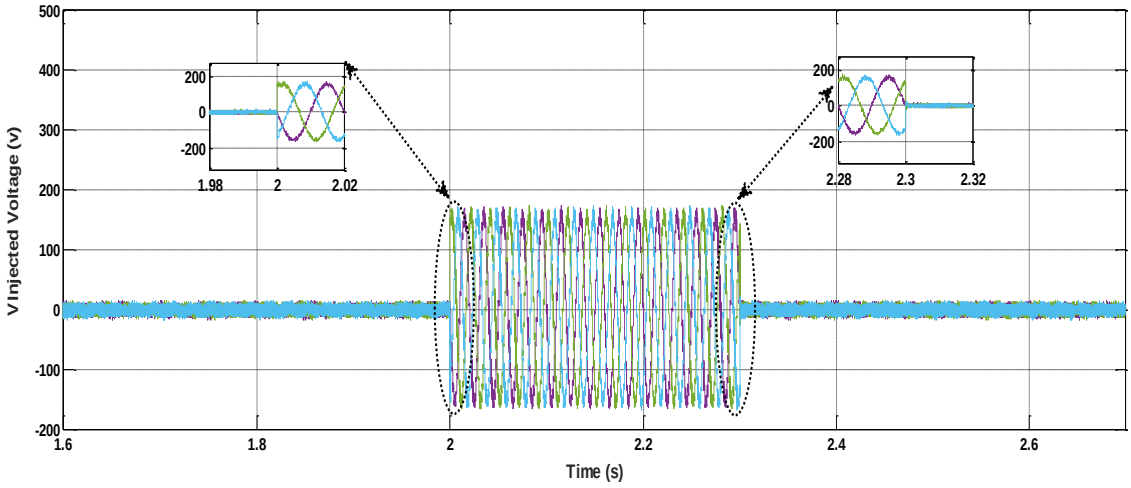
3.1. Voltage sag

This phenomenon is applied between [2-2.3] (s), where the voltage magnitude is selected 50% equivalent to 0.5 pu in the three phases. Figure 5 shows waveforms of the source, injected and the load voltages. As illustrated in the Figure 5, the SAPF has injected the complementary voltage of 0.5 pu during the specified period [2-2.3] (s) of the three phases in the same direction of the source and load voltages. In addition, the curves of the injected currents of the SOFC, and its DC-DC converters are viewed in the Figure 5.

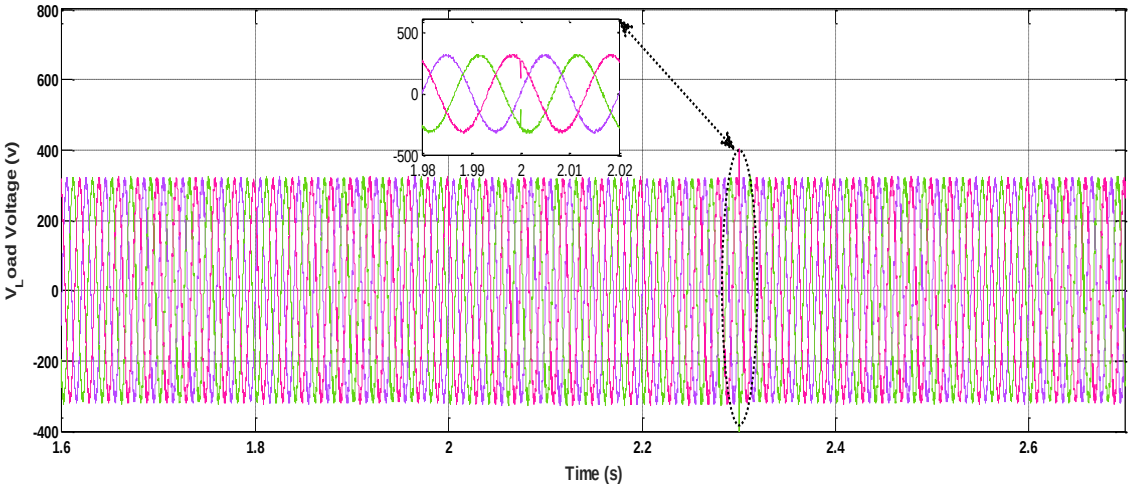
In normal mode, the SAPF necessitate a constant DC voltage of 750V DC across the capacitance equivalent to the input voltage of the inverter 380V AC. Two stage DC-DC boost converters are sized to step up the SOFC voltage to the DC link reference voltage value, where the first boost converter extract the maximum power of the SOFC through the MPPT controller, whereas the second is a regulated output voltage to maintain the dc link voltage constant as shown in Figure 6. As observed, during the applied sag voltage, currents of the SOFC conversion chain have increased because the DC link capacitance has intervened to compensate the sag voltage disturbance as viewed in Figure 7. Therefore, the capacitance is recharged afterward through the generated energy of the SAPF with the SOFC. Figure 8 represents the active power of the SOFC, which is close to the demanded power by the SAPF to compensate the capacitance energy, taking into consideration converter losses due to the switching devices and resistive elements.



(a)



(b)



(c)

Figure 5. Case 1-balanced voltage sag: (a) grid voltages, (b) injected voltage (c) load voltage

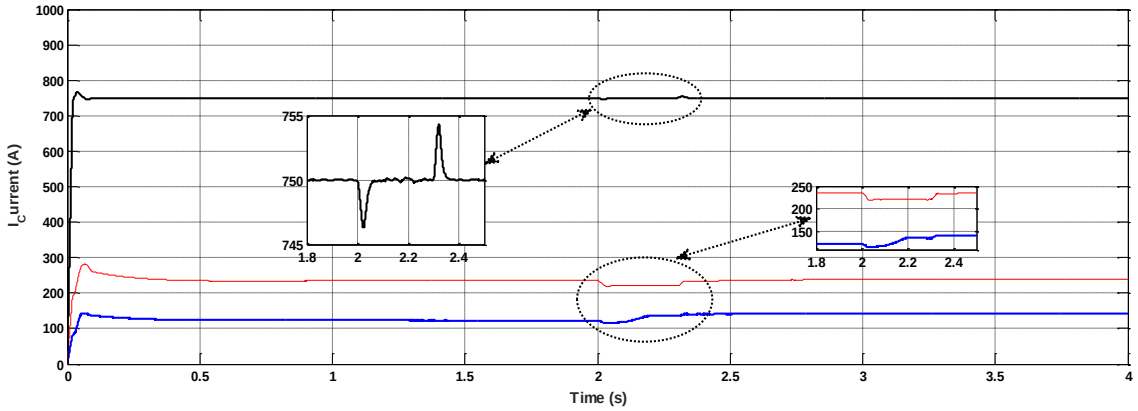


Figure 6. DC voltages of the FC conversion chain in sag voltage case

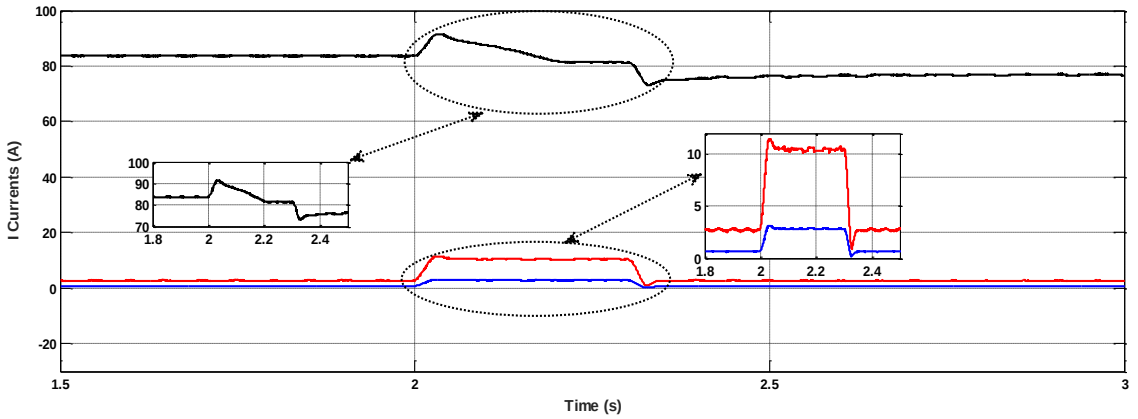


Figure 7. Currents of the FC conversion chain in sag voltage case

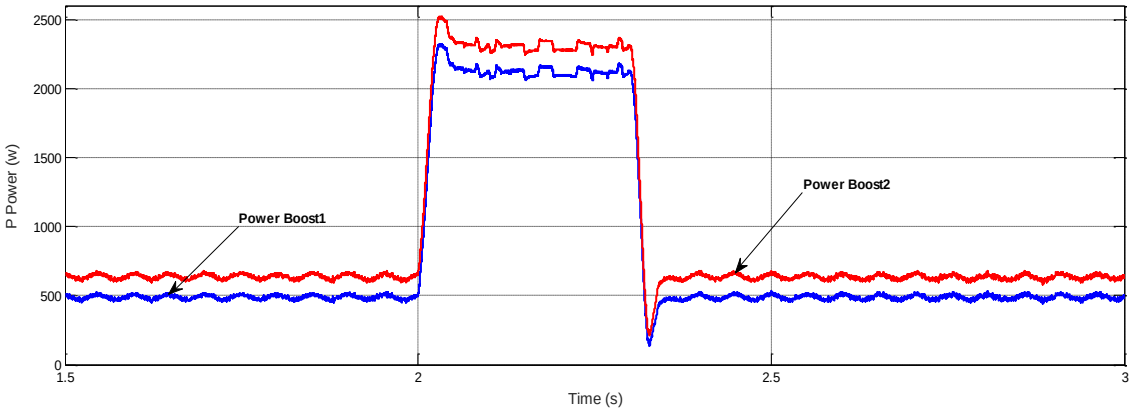
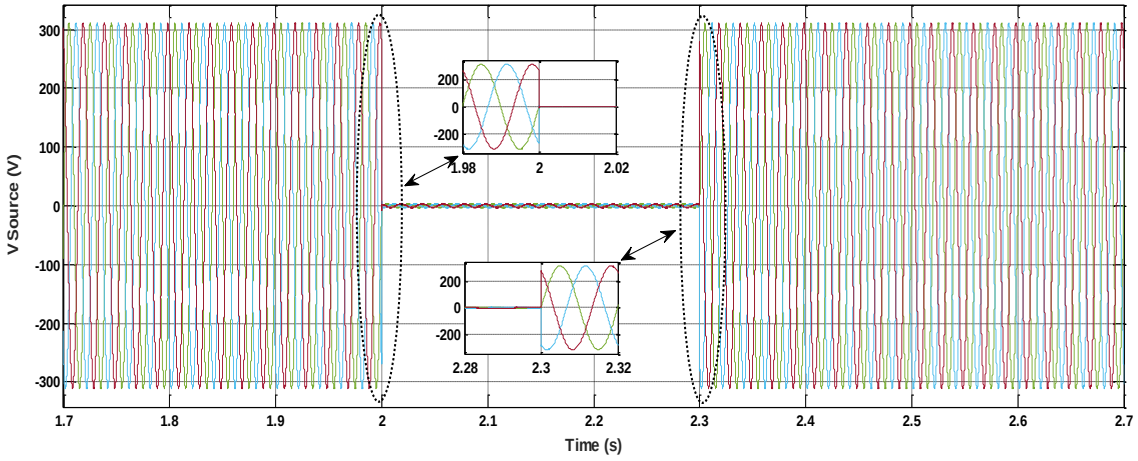


Figure 8. Powers of the FC conversion chain in sag voltage case

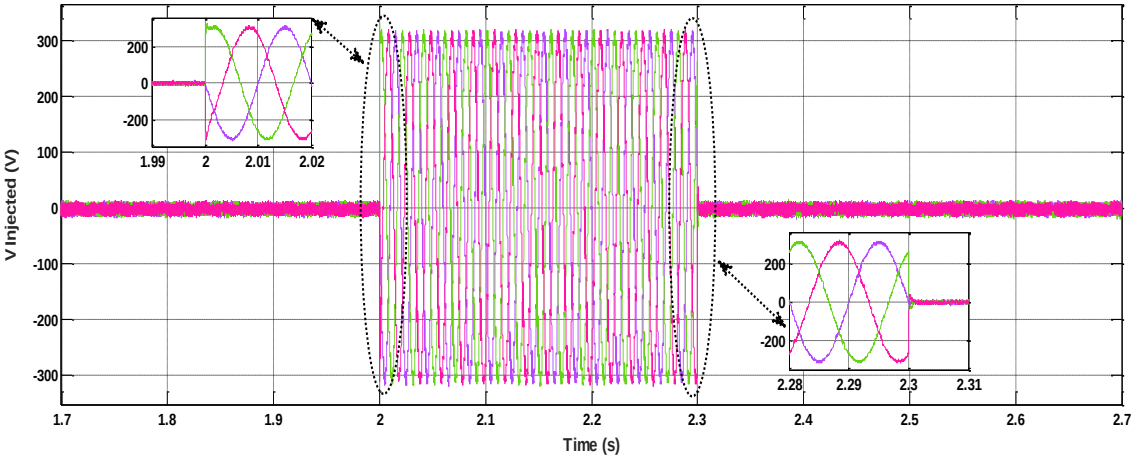
3.2. Voltage interruption

Interruption phenomenon appears when the system voltage decrease with 99% of the reference fundamental value during a specified period do not exceed 60 seconds. In-our case, shown in Figures 9 (a)-(c) respectively the grid voltages, injected voltage and load voltage. The SAPF compensate the lack of energy caused by the interruption of the grid power supply. As seen in previous sag voltage phenomenon, the injected currents of the SOFC conversion chain increased due to discharging the DC link capacitance. In other hand, the injected power was remained constant despite the increasing of currents and decreasing of voltages during the compensation, i.e. at the dc link, the injected power was about [4007.5-4349.5] (W), equivalent to the product

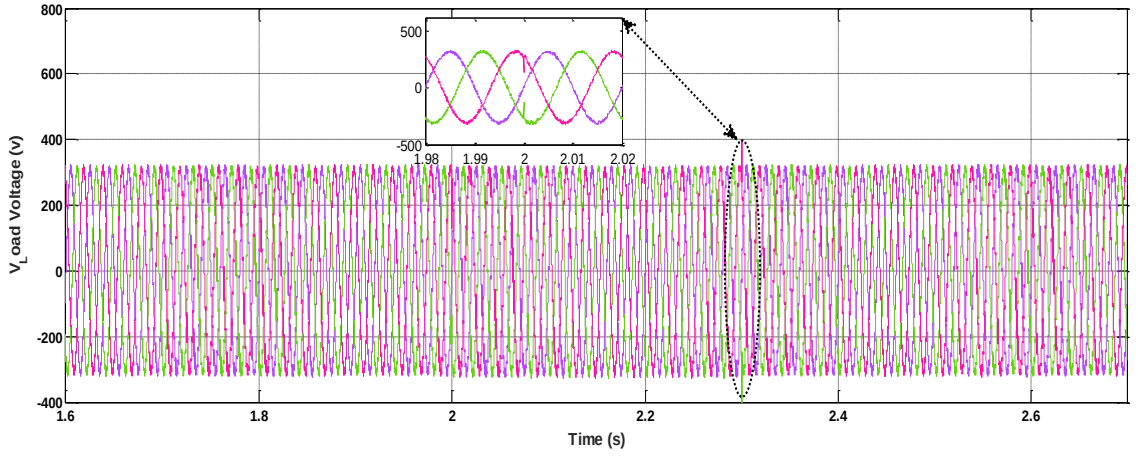
of a current of [5.352-43.85] (A), and a voltage of [748.8-99.19] (Vdc), resulting in a power loss an approximately value of 342 (W). The voltages curves of the source, the injected and the load are shown in Figure 9, where the interruption phenomena is applied and mitigated. Hence, the selected data shown in Figures 10-12 respectively describes the voltages, currents and powers of the two boost converters of the PV conversion chain during normal and perturbed operation modes.



(a)



(b)



(c)

Figure 9. Case 2-voltage interruption: (a) grid voltages, (b) injected voltage (c) load voltage

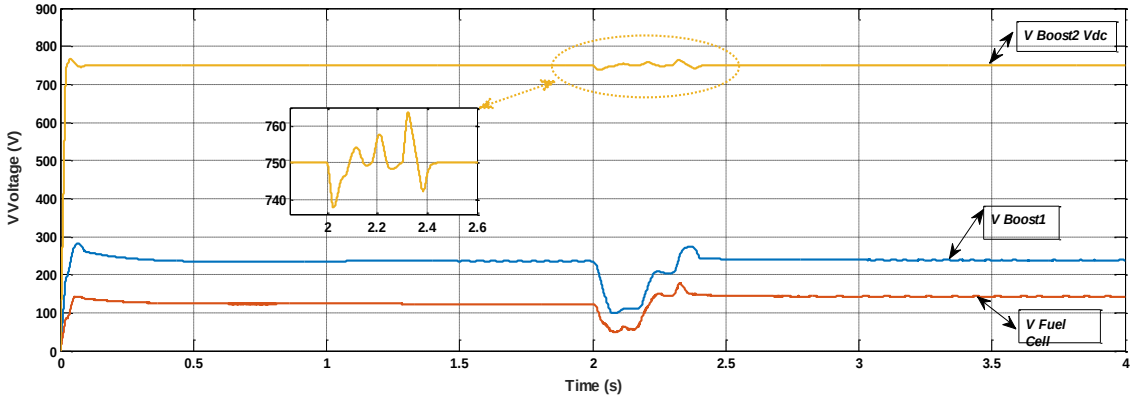


Figure 10. DC voltages of the FC conversion chain in interruption voltage case

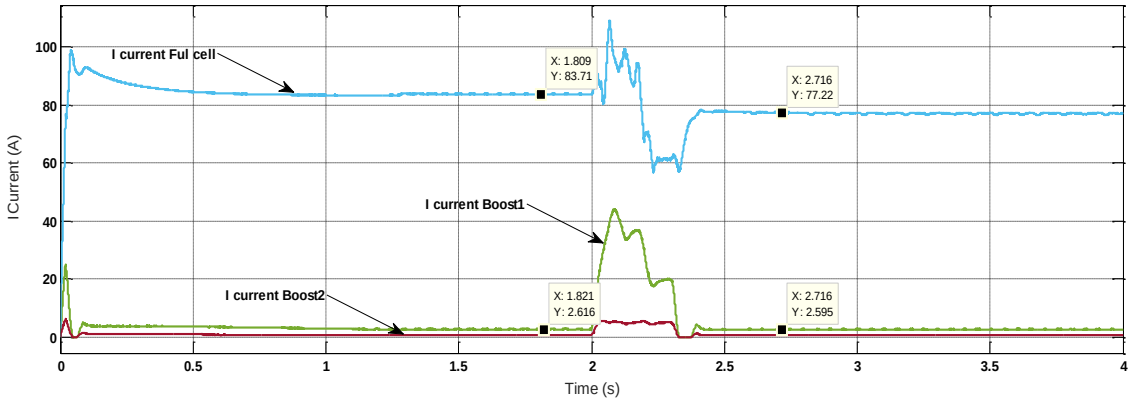


Figure 11. Currents of the FC conversion chain in interruption voltage case

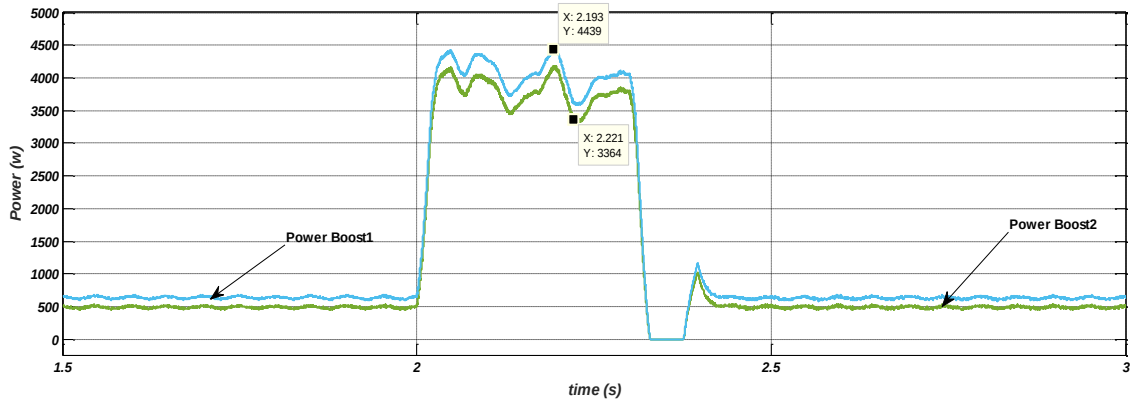
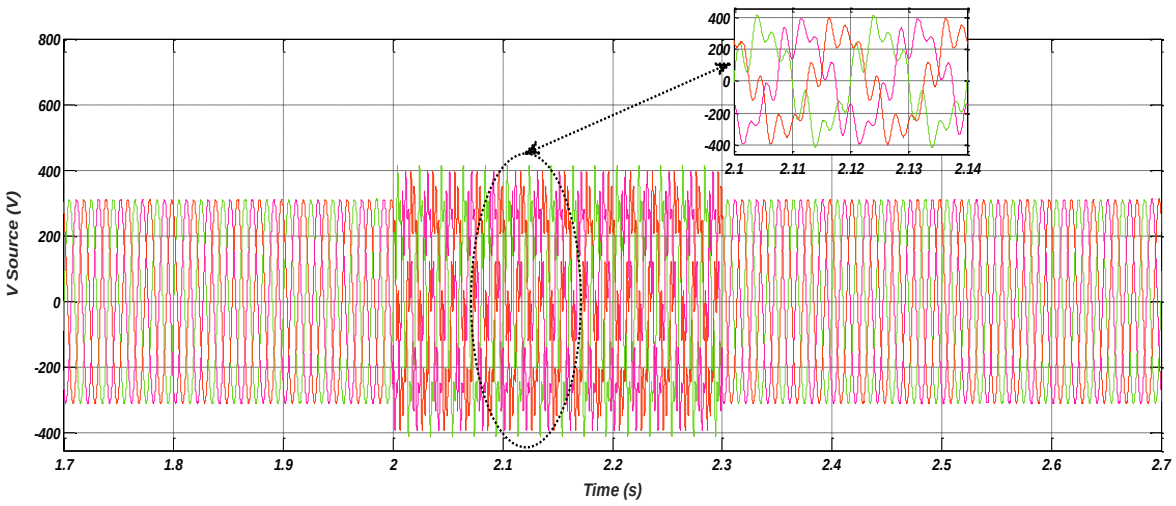


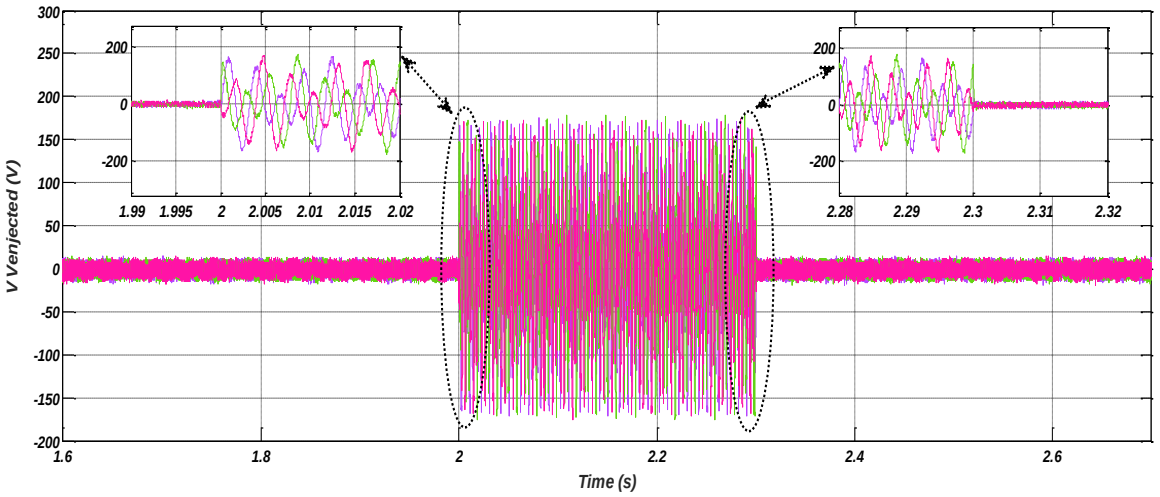
Figure 12. Powers of the FC conversion chain in interruption voltage case

3.3. Harmonics elimination

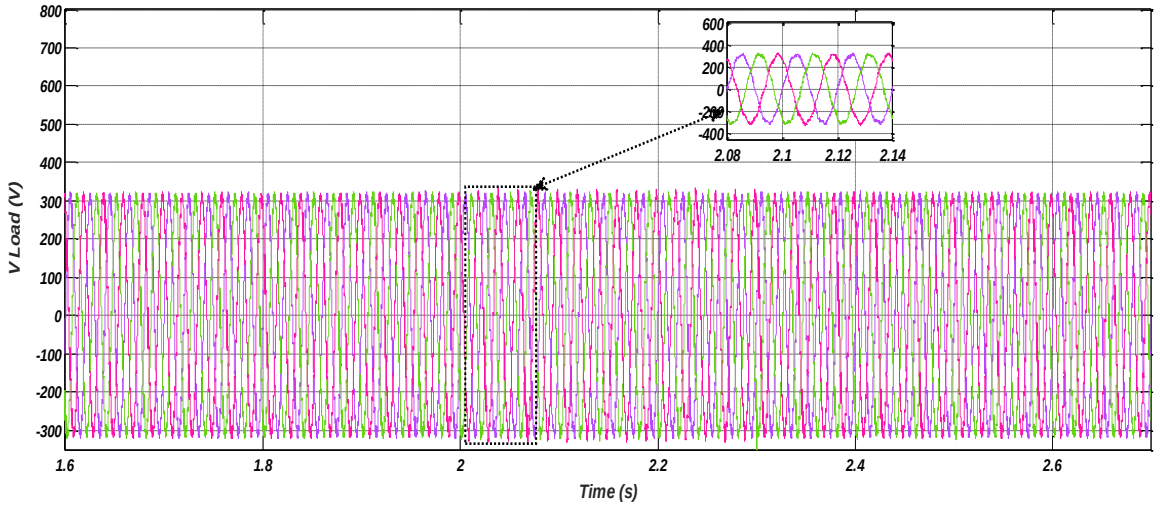
Using the AC programmable source, two main harmonics are generated of the order 5th and 7th with the magnitude and the angle phase of [0.2 pu, 35°] and [0.3 pu, -25°] respectively. At the instance t=2 (s), Figures 13 (a), (b) and c represent the source voltage, injected voltage and load voltage respectively. The FSPA compensate and correct the voltage harmonics by injecting the complementary voltage value through the injection transformer as viewed in the Figure 13. Thus, during the compensation, the total harmonic distortion THD value has ameliorated, where the source THD=10.61% , and the load THD=1.84%. As a remark, the SOFC current did not affected by the applied voltage harmonics, where the voltage harmonics phenomena is applied and mitigated. Hence, the selected data shown in Figures 14-16 respectively describes the voltages, currents and powers of the two boost converters of the PV conversion chain during normal and perturbed operation modes.



(a)



(b)



(c)

Figure 13. Case 3-harmonics elimination: (a) grid voltages, (b) injected voltage (c) load voltage

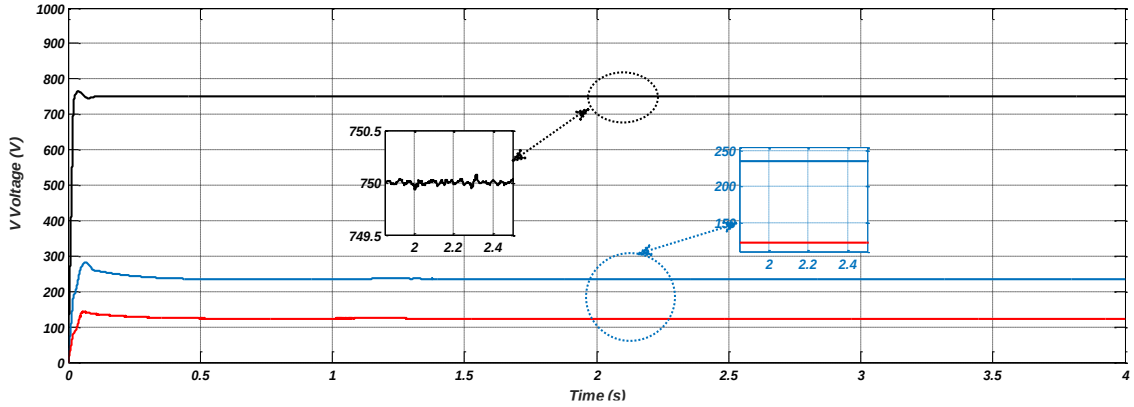


Figure 14. DC voltages of the FC conversion chain in harmonic voltage case

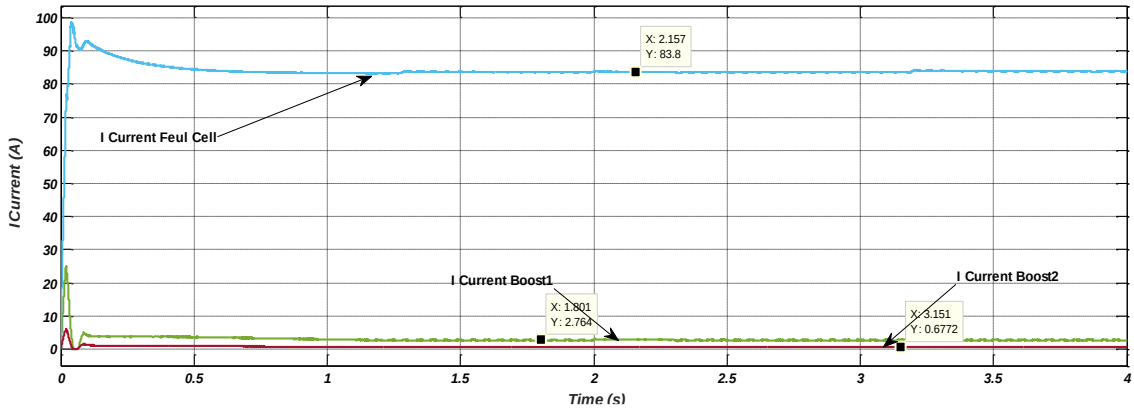


Figure 15. Currents of the FC conversion chain in harmonic voltage case

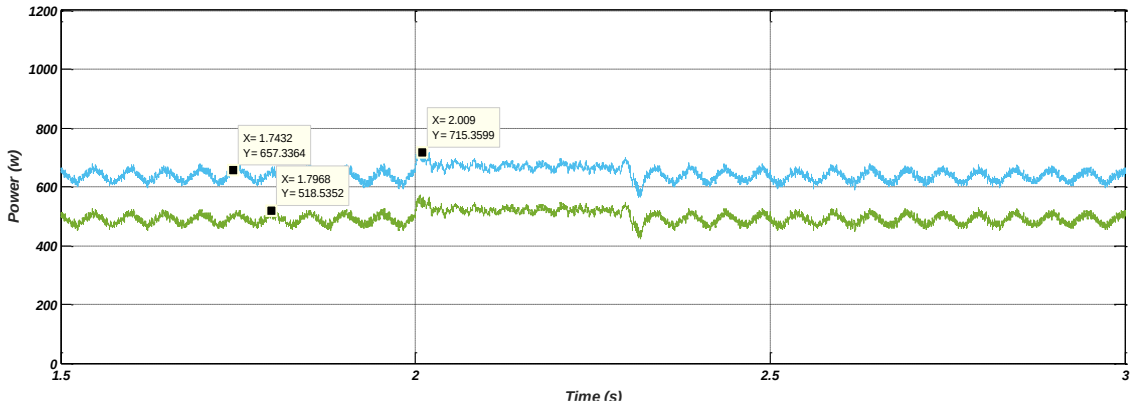


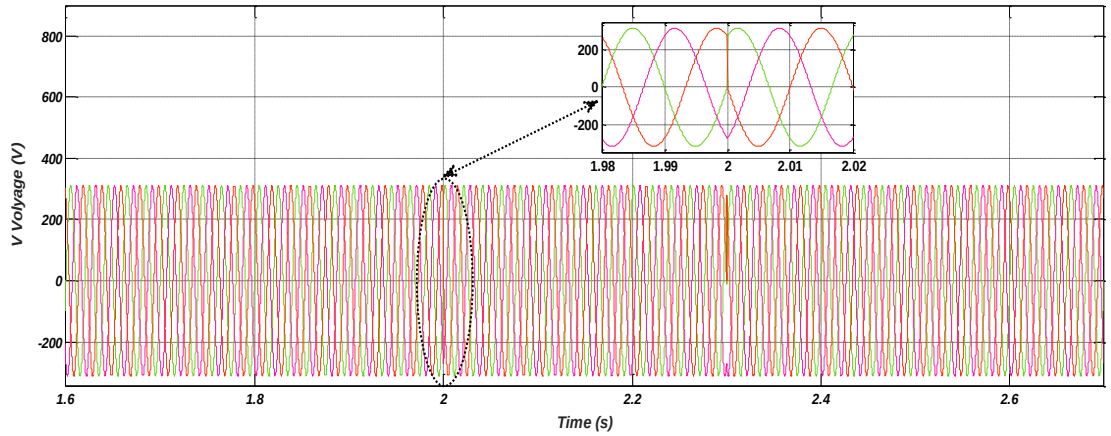
Figure 16. Powers of the FC conversion chain in voltage harmonics case

3.4. Unbalanced voltage

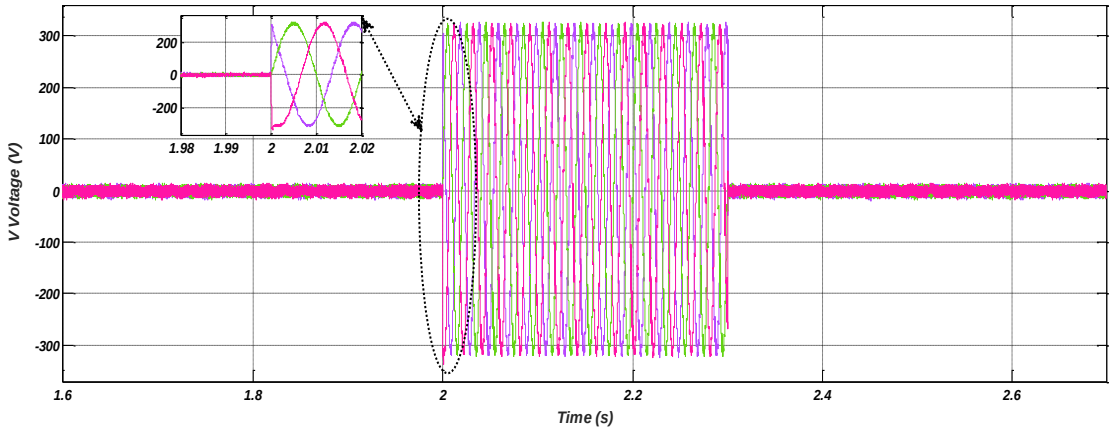
In this case, the AC programmable source is programmed to create a voltage unbalance between the three phases in term of phase angle parameters, where following specifications are used:

- Time variation: Phase
- Type of variation: Step
- Step magnitude: 60°
- Variation timing: [2-2.3] (s)

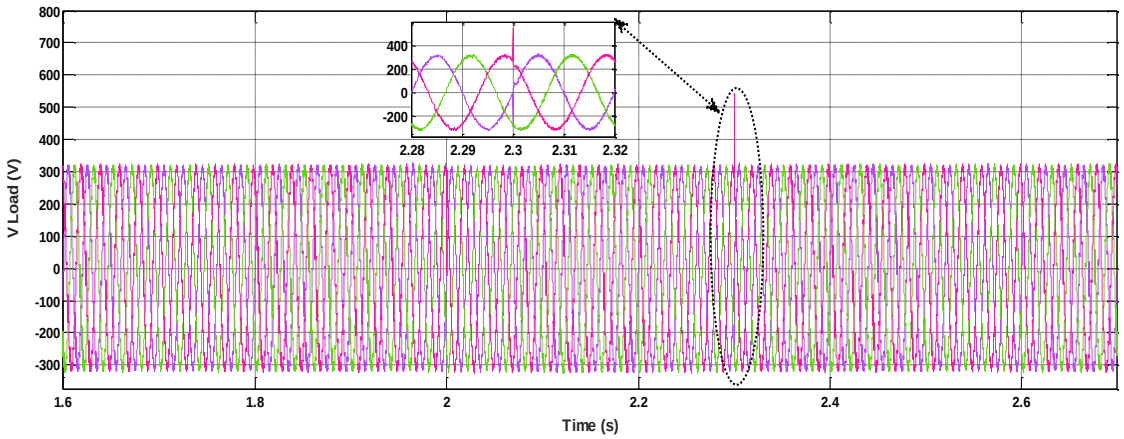
Figures 17 (a), (b) and c represent the source voltage, injected voltage and load voltage respectively. The simulation result of this disturbance is viewed in the Figure 17. As seen, after unbalancing the system voltages with an angle phase of 60°, the SAPF has compensated this disturbance during the specified period between [2-2.3] (s). The estimation of the unbalance value is evaluated by the total of unbalance, which is about 18% in the source side and 0.5% at the load side. Moreover, the load was protected against the applied voltage unbalance, where its voltage waveform was maintained purely sinusoidal. The selected data shown in Figures 18-20 respectively describes the voltages, currents and powers of the two boost converters of the PV conversion chain during normal and perturbed operation modes.



(a)



(b)



(c)

Figure 17. Case 4-unbalanced voltage: (a) grid voltages, (b) injected voltage (c) load voltage

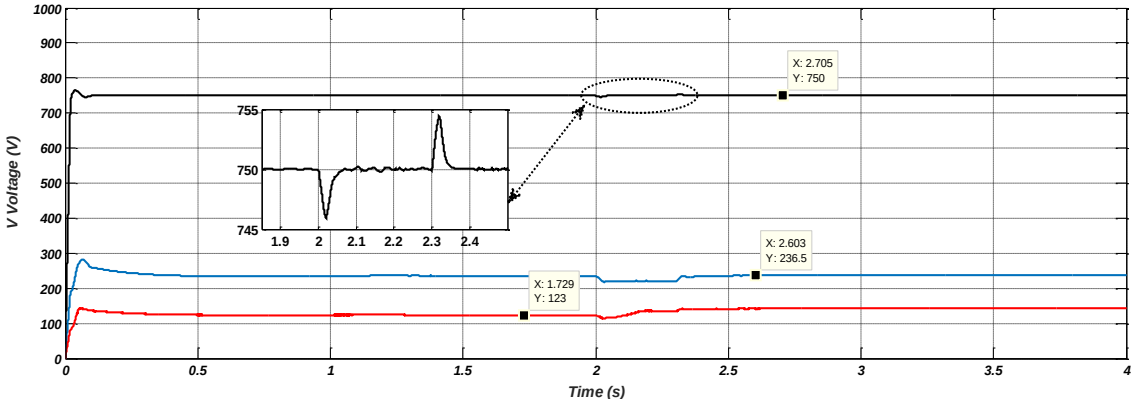


Figure 18. DC voltages of the FC conversion chain in unbalance voltage case

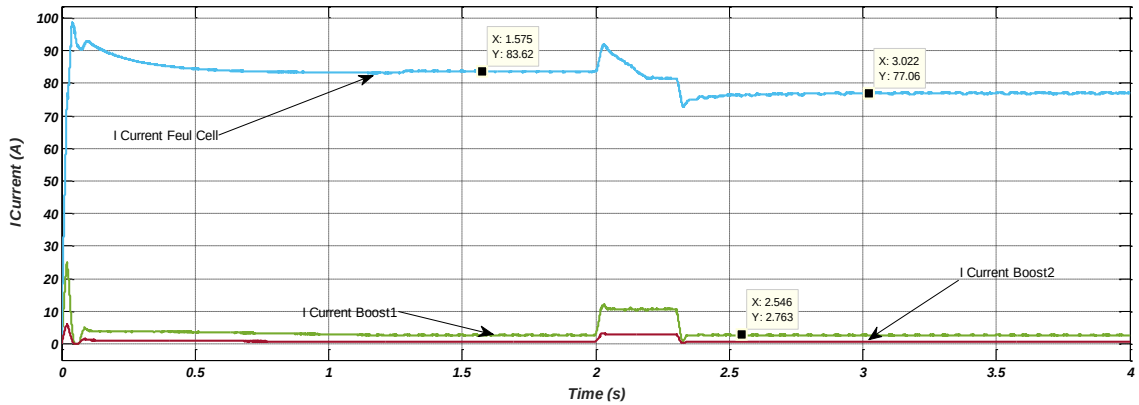


Figure 19. Currents of the FC conversion chain in unbalance voltage case

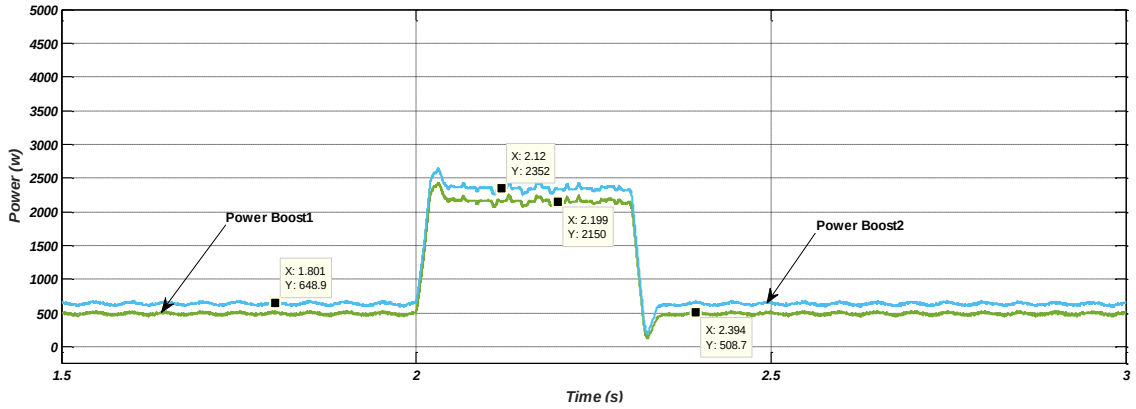


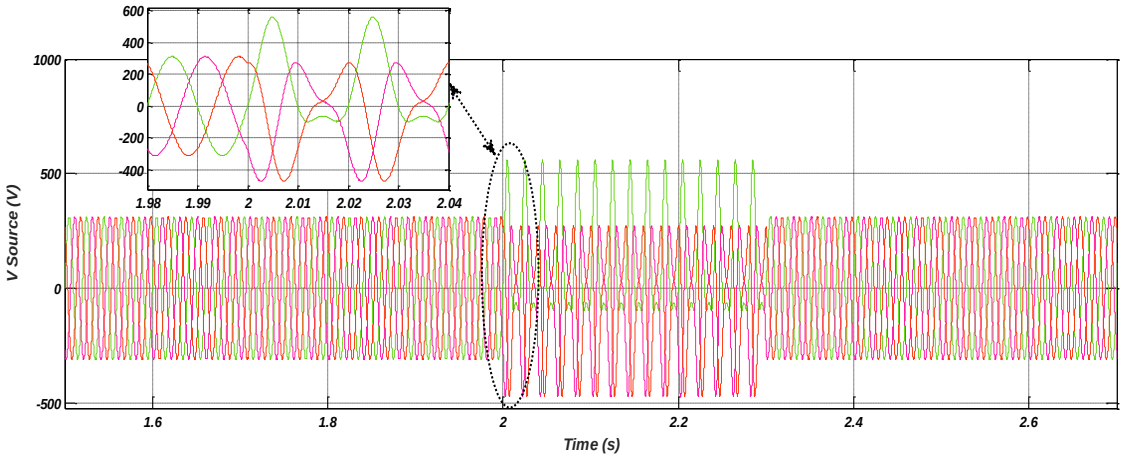
Figure 20. Powers of the FC conversion chain in unbalance voltage case

3.5. Voltage fluctuations

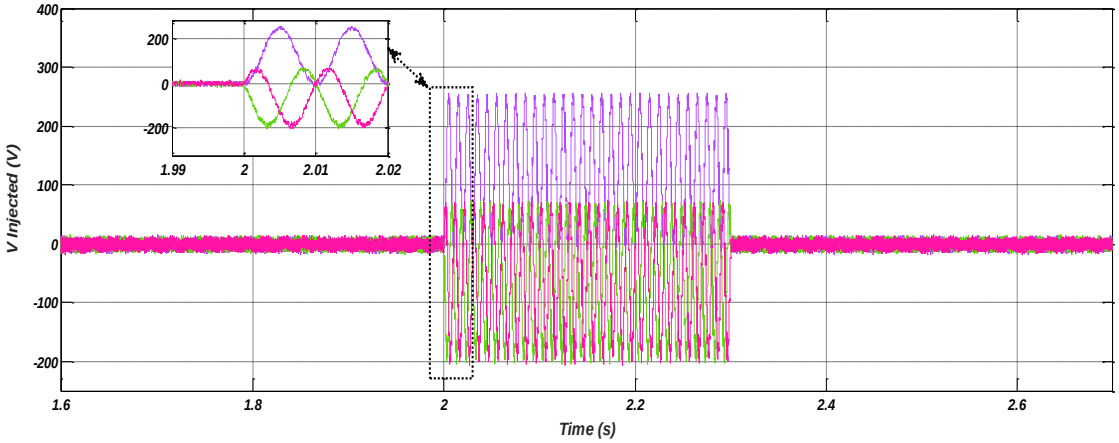
In this phenomenon, the AC programmable source is programmed to create a voltage and frequency disturbances, where following specifications are used:

- Time variation: amplitude
- Type of variation: modulation
- Amplitude: 0.8 pu
- Frequency: 50 Hz
- Variation timing: [2-2.3] (s)

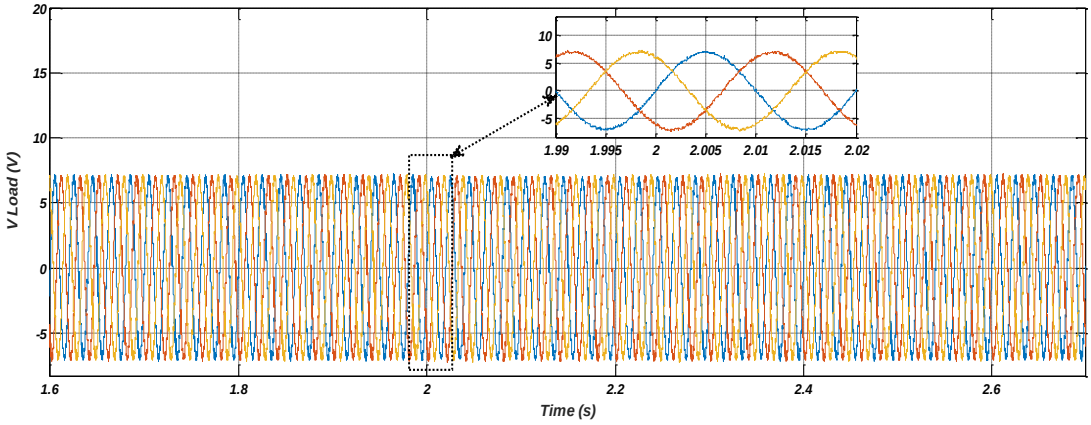
Figures 21 (a), (b) and (c) represent the source voltage, injected voltage and load voltage respectively. Figure 21 illustrated the phenomenon simulation results. As the other created disturbance, the SAPF inject compensating voltage through the injection transformer, which is synchronized and in opposition of phase. The reaction of the SAPF has provided acceptable THD values, where its values at the source side were about 3.54% and 1.54% at the load side. The selected data shown in Figures 22-24 respectively describes the voltages, currents and powers of the two boost converters of the PV conversion chain during normal and perturbed operation modes.



(a)



(b)



(c)

Figure 21. Case 5-voltage fluctuations: (a) grid voltages, (b) injected voltage (c) load voltage

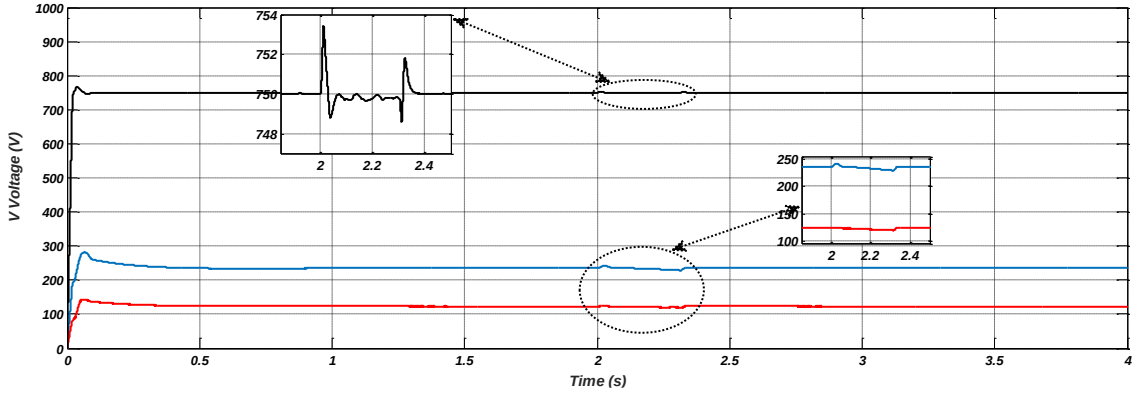


Figure 22. DC voltages of the FC conversion chain in fluctuations voltage case

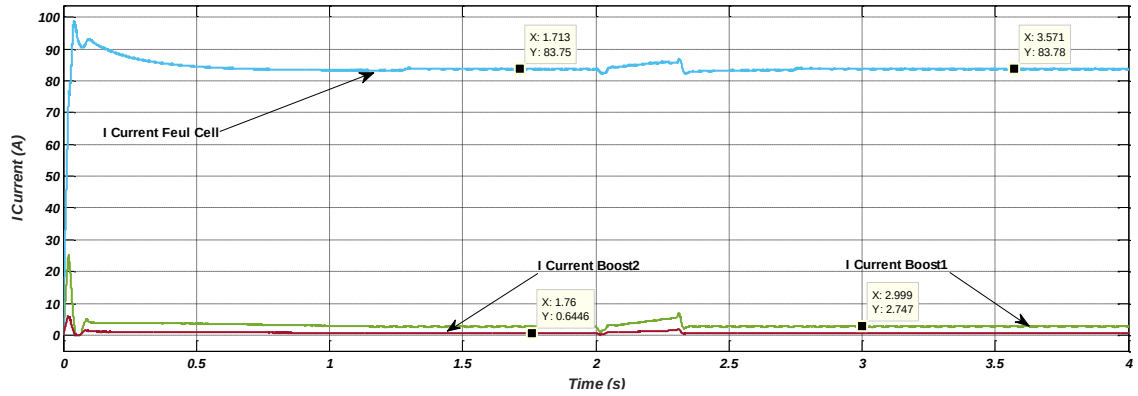


Figure 23. Currents of the FC conversion chain in fluctuations voltage case

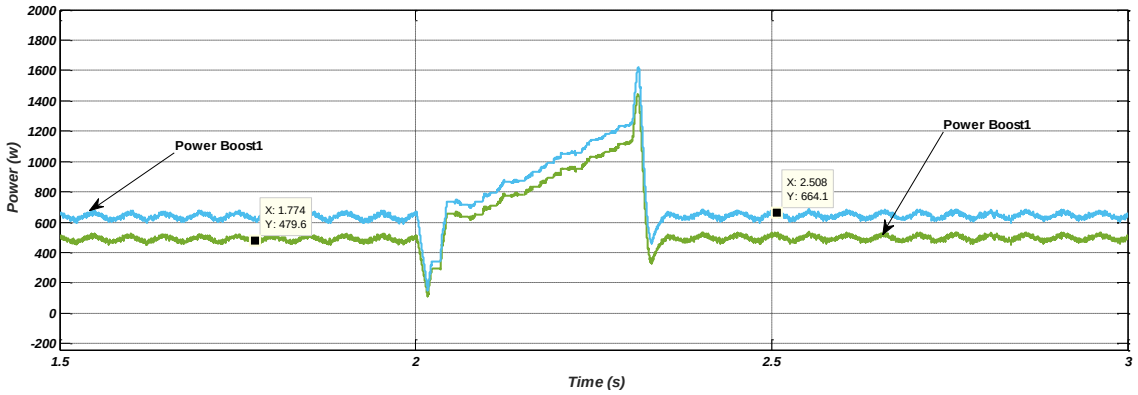


Figure 24. Powers of the FC conversion chain in fluctuations voltage case

4. CONCLUSION

Through this brief study, a SAPF relies on FC source was used in order to mitigate voltage disturbances such as sag-swell and harmonics. In this paper, a conversion chain is connected to the renewable source FC, where the control strategy of the DC side is based on two combined controllers. First, The MPPT controller is applied in the first DC-DC boost converter to extract the maximum power of the FC, while the high side voltage of the second DC-DC converter is maintained constant during the applied disturbances using closed control loops. Exactly, duty cycles performed by the proportional integral PI compensator are adjusted in order to mitigate DC bus variations and extract the maximum by generating PWM signals to the switching devices of the DC-DC converters. Among the obtained results, renewable energies can be an efficient solution to solve power quality issues.

APPENDIX

The DC-DC converters are regulated through either the closed loop control of the output voltage, the closed loop control of the inner current or through a combined current-voltage bi-loop. The (31) and (32) illustrate the control to the output voltage VC and to the inductor current iLof the boost converter:

$$\frac{V_C}{d} = \frac{V_{in}}{RC(1-D)^2} \frac{-s+\frac{R(1-D)^2}{L}}{s^2+\frac{s}{RC}+\frac{(1-D)^2}{LC}} \quad (31)$$

$$\frac{i_L}{d} = \frac{V_{in}}{L(1-D)} \frac{s+\frac{2}{RC}}{s^2+\frac{s}{RC}+\frac{(1-D)^2}{LC}} \quad (32)$$

For the boost mode, the output voltage V_{DC}=750V, where the battery voltage varies between the cut-off voltage 350 V, the nominal voltage 400V, and the fully charged voltage 450V. Thus, the duty cycle in this mode can be calculated as:

$$\begin{cases} d_{min} = 1 - {V_{full\ charge}}/{V_{DC}} \\ d_{Nom} = 1 - {V_{Nom}}/{V_{DC}} \\ d_{max} = 1 - {V_{cut-off}}/{V_{DC}} \end{cases}$$

$$\begin{cases} d_{min} = 1 - {V_{OC}}/{V_{DC}} \\ d_{max} = 1 - {V_{MPPT}}/{V_{DC}} \end{cases}$$

Table 2. System parameters

System parameters	Value
Power system	
Grid voltage	220V
Frequency	50Hz
Line impedance	$0{,}0001 + \text{j}19.5\text{e}^{-6}\Omega$
Load	Three-phase $R_{AC} = 50\Omega$, $L_{AC} = 1$ mH
SAPF	
DC link voltage	$750\ V$
DC link capacitor	$3300\ e^{-6}F$
PWM switching	$20\ KHz$
Connection filter of series filter (RLC)	$R = 0.0020\ \Omega$, $L = 1.4814e-04F$, $C = 5.2773e-05F$
DC-DC boost1	
L	$0.716e-6H$
C	$2200e-6F$
DC-DC boost2	
L	$0.2e-3H$
C	$0.02e-06F$
Loop current	
PI controller	
K_P	0.97
K_I	33
Loop voltage	
PI controller	
K_P	0.97
K_I	55
Fuel cell stack	
Nominal power	2x3.195 kW
Nominal current	30 A
Nominal voltage	106.5 V
Maximum power	3.481 kW
Maximum power point current	33.2 A
Maximum power point voltage	104.86 V
Stack efficiency	52%

ACKNOWLEDGEMENTS

At the end of this work, I thank all doctor colleges and professors who participated in this work with their information's and who helped me as possible. Smart grid and renewable energies laboratory (SGRE-Lab) for providing all necessary equipment and material and moral assistance.

REFERENCES

[1] A. Prasai and D. M. Divan, "Zero-energy sag correctors-optimizing dynamic voltage restorers for industrial applications," *IEEE Transactions on Industry Applications*, vol. 44, no. 6, pp. 1777-1784, 2008.
[2] H. Akagi, E. H. Watanabe, and M. Aredes, "Instantaneous power theory and applications to power conditioning," John Wiley & Sons, 2017.
[3] E. C. dos Santos, C. B. Jacobina, J. A. A. Dias and N. Rocha, "Single-phase to three-phase universal active power filter," *IEEE Transactions on Power Delivery*, vol. 26, no. 3, pp. 1361-1371, 2011.
[4] A. B. Abdelkader O. Abdelkhalek and A. Allali, "Experimental validation of single phase series active power filter using fuzzy control technique," *International Journal of Power Electronics and Drive Systems*, vol. 9, no. 2, pp. 591-601, 2018.
[5] A. Meena, S. Islam, S. Anand, Y. Sonawane and S. Tungare, "Design and control of single-phase dynamic voltage restorer," *Sadhana*, vol. 42, no. 8, pp. 1363-1375, 2017.
[6] R. Lawrence, "Power quality and electrical reliability: Where does the responsibility lie," *Energy Engineering*, vol. 106, no. 6, pp. 23-33, 2009.
[7] H. Akagi and K. Isozaki, "A hybrid active filter for a three-phase 12-pulse diode rectifier used as the front end of a medium-voltage motor drive," *IEEE Transactions on Power Electronics*, vol. 27, no. 1, pp. 69-77, 2012.
[8] A. Chaoui, J. P. Gaubert, F. Krim and G. Champenois, "PI controlled three-phase shunt active power filter for power quality improvement," *Electric Power Components and Systems*, vol. 35, no. 12, pp. 1331-1344, 2007.
[9] M. J. Newman, D. G. Holmes, J. G. Nielsen and F. Blaabjerg, "A dynamic voltage restorer (DVR) with selective harmonic compensation at medium voltage level," *38th IAS Annual Meeting on Conference Record of the Industry Applications Conference*, vol. 2, pp. 1228-1235, 2003.
[10] F. B. Ajaei, S. Afsharnia, A. Kahrobaeian and S. Farhangi, "A fast and effective control scheme for the dynamic voltage restorer," *IEEE Transactions on Power Delivery*, vol. 26, no. 4, pp. 2398-2406, 2011
[11] F. A. L. Jowder, "Design and analysis of dynamic voltage restorer for deep voltage sag and harmonic compensation," *IET Generation, Transmission & Distribution*, vol. 3, no. 6, pp. 547-560, 2009.
[12] A. Pandey, R. Agrawal, R. S. Mandloi and B. Sarkar, "Sliding mode control of dynamic voltage restorer by using a new adaptive reaching law," *Journal of The Institution of Engineers: Series B*, vol. 98, no. 6, pp. 579-589, 2017.
[13] A. Telli and S Barkat, "Distributed grid-connected SOFC supporting a multilevel dynamic voltage restorer," *Energy Systems*, vol. 10, pp. 461-487, 2018.
[14] M. Azri, N. H. Abu Khanipah, Z. Ibrahim and N. Rahim, "Fuel cell emulator with MPPT Technique and boost converter," *International Journal of Power Electronics and Drive Systems*, vol. 8, no. 4, pp. 1852-1862, 2017.
[15] A. K. Saha, S. Chowdhury, S. P. Chowdhury and Y. H. Song, "Application of solid-oxide fuel cell in distributed power generation," *IET Renew. Power Gen.*, vol. 1, no. 4, pp. 193-202, 2007.
[16] B. Slimane, A. Othmane and B. Abdallah, "Unified power quality conditioner supplied by fuel cell system via SEPIC converter," *International Journal of Power Electronics and Drive Systems*, vol. 10, no.1, pp. 178-194, 2019.
[17] E. M. Stewart, R. Tumilty, J. Fletcher, A. Lutz, G. Ault and J. McDonald, "Analysis of a distributed grid-connected fuel cell during fault conditions," *IEEE Transactions on Power Syst.*, vol. 25, no. 1, pp. 497-505, 2010.
[18] S. A. Taher and S. Mansouri, "Optimal PI controller design for active power in grid-connected SOFC DG system," *International Journal of Electrical Power & Energy Systems*, vol. 60, pp. 268-274, 2014.
[19] A. Chandra, B. Singh, B. N. Singh and K. Al-Haddad, "An improved control algorithm of shunt active filter for voltage regulation, harmonic elimination, power-factor correction, and balancing of nonlinear loads," *IEEE Transactions on Power Electronics*, vol. 15, no. 3, pp. 495-507, 2000.

BIOGRAPHIES OF AUTHORS



Abdallah Ben Abdelkader received the L. Sc. degree in electrical engineering from Bechar University, Bechar, Algeria, in 2006 and M.Sc. degree in electrical engineering from University of Sciences and Technology of Oran (USTO) Algeria, in 2013, respectively, where he has been working toward the doctoral degree in the Department of Electrical Engineering, 2013. He is currently a research member of Smart Grids and Renewable Energies Lab, Department of Electrical Engineering, Tahri Mohammed University Bechar, Algeria. His main research activity is focused on FACTS technology, power system control, and optimal power dispatch.



Othmane Abdelkhalek was born in Taghit, Bechar, Algeria, in 1976. He graduated from the University of Tahri Mohamed, Faculty of Electrical Engineering in Bechar, Algeria in 2001. He received the engineering degree from Bechar University Center in 2001, the magister degree from Sidi-Bel-Abbes University in 2004 and the doctorate from the University of Bechar in 2010. His research area interests are power electronic, power quality, active filtering, DVR, UPQC, control, digital control, load flow optimization. He is working on low voltage direct current micro-grid, and renewable energies integration in island DC micro-grids.
E-mail : othmane.Abdelkhalek@labrier-univ-bechar.dz



Youssef Mouloudi received the state engineer degree in electrical engineering in 2006 from the University of Bechar and the M.S. degree in 2009 from Bechar University, Algeria. He is currently a PhD. student of the Faculty Technology, University of Bechar, Algeria. He is working at SONELGAZ "Algerian Electrical Society" since 1995. His areas of interest are FACTS systems, power filters, applications of power electronics, and stability improvement. Correspondence address: Dept. Science and Technology "Electrical Engineering", Faculty of Technology, Bechar University, BP 417, 08000 Bechar, Algeria. E-mail: mouloudiyoussef@yahoo.fr



Hartani Mohamed Amine was born in Beni-ounif, Bechar, Algeria, in 1993. He graduated from the Faculty of Electrical Engineering, University of Tahri Mohamed-Bechar, Algeria in 2012. He received license degree in electrical engineering from Tahri Mohamed University-Bechar, Algeria in 2015. After master degree in control and monitoring of electrical machines from the same university in 2017. Now, he is a doctoral student in electrical engineering in collaboration with Ahmed Draya University, Adrar, Algeria and Tahri Mohamed University, Bechar, Algeria. His researches focus on the energy management of island and remote areas, integration of renewable energies in DC smart Microgrids, autonomous and hybrid systems based on renewable energies and storage devices, optimization methods, classical control strategies and genetic algorithms.
E-mail: hartani_mohamed@univ-adrar.dz



Benabid Slimane graduated from the Faculty of Technology, University of Bechar, Algeria, in 2005. He received magister degree in electrical engineering from the University of Bechar, Algeria, in 2009, where he has been working toward the doctoral degree at the Department of Electrical Engineering in 2010. He is currently a research member at the Smart Grids and Renewable Energies Lab, Department of Electrical Engineering Tahri Mohammed University Bechar, Algeria. His research interests concern: FACTS Technology, artificial intelligence, power system control and optimal power dispatch.